Journal of Atmospheric and Solar-Terrestrial Physics 167 (2018) 66–73

Contents lists available at ScienceDirect

Journal of Atmospheric and Solar-Terrestrial Physics

journal homepage: www.elsevier.com/locate/jastp

Making limb and nadir measurements comparable: A common volume study of PMC brightness observed by Odin OSIRIS and AIM CIPS

Susanne Benze [a,b,*], Jörg Gumbel [b], Cora E. Randall [a,c], Bodil Karlsson [b], Kristoffer Hultgren [b], Jerry D. Lumpe [d], Gerd Baumgarten [e]

[a] Laboratory for Atmospheric and Space Physics, Univ. Colorado, Boulder, CO, USA
[b] Department of Meteorology, Stockholm University, Stockholm, Sweden
[c] Department of Atmospheric and Oceanic Sciences, Univ. Colorado, Boulder, CO, USA
[d] Computational Physics, Inc., Boulder, CO, USA
[e] Leibniz-Institute of Atmospheric Physics at Rostock University, Kühlungsborn, Germany

ARTICLE INFO

Keywords:
Polar mesospheric cloud
OSIRIS
CIPS
Common volume
Limb
Nadir

ABSTRACT

Combining limb and nadir satellite observations of Polar Mesospheric Clouds (PMCs) has long been recognized as problematic due to differences in observation geometry, scattering conditions, and retrieval approaches. This study offers a method of comparing PMC brightness observations from the nadir-viewing Aeronomy of Ice in the Mesosphere (AIM) Cloud Imaging and Particle Size (CIPS) instrument and the limb-viewing Odin Optical Spectrograph and InfraRed Imaging System (OSIRIS). OSIRIS and CIPS measurements are made comparable by defining a common volume for overlapping OSIRIS and CIPS observations for two northern hemisphere (NH) PMC seasons: NH08 and NH09. We define a scattering intensity quantity that is suitable for either nadir or limb observations and for different scattering conditions. A known CIPS bias is applied, differences in instrument sensitivity are analyzed and taken into account, and effects of cloud inhomogeneity and common volume definition on the comparison are discussed. Not accounting for instrument sensitivity differences or inhomogeneities in the PMC field, the mean relative difference in cloud brightness (CIPS - OSIRIS) is $-102 \pm 55\%$. The differences are largest for coincidences with very inhomogeneous clouds that are dominated by pixels that CIPS reports as non-cloud points. Removing these coincidences, the mean relative difference in cloud brightness reduces to $-6 \pm 14\%$. The correlation coefficient between the CIPS and OSIRIS measurements of PMC brightness variations in space and time is remarkably high, at 0.94. Overall, the comparison shows excellent agreement despite different retrieval approaches and observation geometries.

1. Introduction

Polar mesospheric clouds (PMCs), also called NoctiLucent Clouds (NLCs), are thin water ice clouds that form in the polar summer mesopause region. Since these clouds are sensitive to changes in mesospheric temperature and water vapor they have been discussed as possible indicators of global climate change in the upper atmosphere (e.g., Thomas, 1996; Thomas et al., 2003; von Zahn, 2003; Schröder, 2003; Lübken et al., 2009). However, mesospheric temperature and water vapor also depend strongly on middle atmosphere dynamics, which are controlled by wave - mean flow interactions (e.g., Andrews et al., 1987; Shepherd, 2000; Siskind et al., 2012). A third controlling factor of PMC variability is solar variations (e.g., Garcia, 1989; DeLand et al., 2003; Robert et al., 2010).

PMCs have been observed from the ground since 1885 (Backhouse, 1885; Leslie, 1885; Jesse, 1885). The first observation from satellite was reported in 1972 (Thomas and Donahue, 1972), and regular satellite observations started in 1978 (e.g., Thomas et al., 1991). Most satellite observations of PMCs are based on serendipitous measurements by instruments originally intended to investigate other atmospheric phenomena. For PMC investigations mostly polar orbiting satellites are used, which have regularly spaced longitude coverage over the entire planet. The most common observation techniques from these satellites include measurement of 1) nadir backscattering in the UV, e.g., the Solar Backscattered Ultraviolet (SBUV) series of instruments (e.g., Thomas et al., 1991; DeLand et al., 2003) and the Aeronomy of Ice in the Mesosphere

* Corresponding author. Department of Meteorology, Stockholm University, Stockholm, Sweden.
E-mail address: susanne.benze@misu.su.se (S. Benze).

https://doi.org/10.1016/j.jastp.2017.11.007
Received 20 June 2017; Received in revised form 22 October 2017; Accepted 13 November 2017
Available online 16 December 2017

(AIM) Cloud Imaging and Particle Size (CIPS) experiment (Russell et al., 2009); 2) limb scattering from UV to IR, e.g., the Solar Mesosphere Explorer (SME) (Thomas, 1984), the Student Nitric Oxide Explorer (SNOE) (Bailey et al., 2005), the Michelson Interferometer for Passive Atmospheric Sounding (MIPAS) (García-Comas et al., 2016), and the Odin Optical Spectrograph and InfraRed Imaging System (OSIRIS) (Llewellyn et al., 2004); and 3) solar occultation from the UV to the IR, e.g., the Halogen Occultation Experiment (HALOE) (Hervig and Siskind, 2006), the Polar Ozone and Aerosol Measurement (POAM) instruments (Lumpe et al., 2008), and the AIM Solar Occultation For Ice Experiment (SOFIE) (Gordley et al., 2009).

Each satellite observation technique has its own unique advantages and disadvantages. For example, nadir- and limb-viewing instruments that measure scattered radiation sample nearly the entire summer polar region each day, providing between a few hundred and several thousand potential PMC measurements. Solar occultation instruments in high inclination orbits provide only 14–15 observations in the polar region of each hemisphere per day, all located on one latitude circle. Both solar occultation and limb scattering instruments resolve vertical features of clouds with a resolution of typically 1–3 km, whereas nadir observations of PMCs do not provide any vertical profiles.

Combining and co-analyzing observations from two instruments with different observation geometries/techniques potentially yields more information than each one instrument can provide. For example, PMC observations retrieved from limb viewing instruments have very good vertical resolution of cloud structure, but are complicated by inhomogeneity of clouds along the line-of-sight. A nadir instrument that provides information on the inhomogeneities on a fine enough scale can potentially improve the limb retrieval results. Combining observations this way is challenging because (1) a common cloud measurement parameter that combines two fundamentally different observations and geometries must be defined; (2) a common volume of atmosphere that both instruments sample must be chosen; and (3) the uncertainties that arise from errors in both instruments and from the assumptions made for the choice of common volume must be quantified. Current examples of such efforts are comparisons of PMC observations from CIPS and SOFIE on the AIM satellite (Bailey et al., 2015) and ground-based Lidar and AIM CIPS (Baumgarten et al., 2012). This work combines and compares PMC common volume observations from instruments on two different satellites with different observation geometries for the first time.

AIM/CIPS was launched in April 2007 and is still operational at the time of this study. AIM is the first satellite with the primary purpose to observe PMCs. CIPS is a panoramic Ultra Violet (UV) nadir imager operating at 265 ± 7 nm (Russell et al., 2009). It consists of four wide-angle cameras that together cover an area of about 2000 km along the orbit track and about 1 000 km across the orbit track (McClintock et al., 2009). This results in complete polar coverage at latitudes between ~68° and 84°–89° in either hemisphere during the summer season, and very good spatial coverage for lower latitudes in the PMC region. Because of long-term drift of the orbit plane, the maximum latitude reached has increased over time from about 84° to 89°. Multiple exposures of individual clouds from different scattering angles (SCAs) are used to measure the phase function (Bailey et al., 2009), which enables retrievals of PMC ice water content and ice particle mode radius in addition to cloud directional albedo. The CIPS operational data product has a horizontal resolution of 25 km^2, which is unprecedented for satellite observations of PMCs. As a nadir imager, CIPS integrates over vertical columns, and therefore does not resolve vertical structures. In this study CIPS v4.20 level 2 cloud albedo is used. For an in-depth description of the CIPS algorithm, error analysis, and cloud detection sensitivity the reader is referred to Lumpe et al. (2013). Previous validation efforts comparing CIPS v3.20 level 1a data to PMC results from the SBUV/2 instruments are presented by Benze et al. (2009, 2011).

OSIRIS was launched on the Odin satellite in February 2001 and is still operational at the time of this study. Odin is a joint project of radio astronomers and atmospheric scientists; the goals of the atmospheric mission are to better understand stratospheric and mesospheric ozone, summer mesospheric science, and coupling of atmospheric regions (Murtagh et al., 2002). OSIRIS measures sunlight scattered from the Earth's limb between 275 nm and 815 nm with a spectral resolution of about 1 nm (Llewellyn et al., 2004). The spectral structure of the scattered light enables retrieval of PMC brightness, particle sizes, and ice water content (von Savigny et al., 2005; Karlsson and Gumbel, 2005; Hultgren and Gumbel, 2014). In the current study, we use the shortest wavelengths available from OSIRIS, integrating over a spectral interval 276.3–278.3 nm. The vertical field of view is 1 km, the field of view across track is 30 km. As a limb-viewing instrument, OSIRIS integrates over a horizontal line-of-sight and therefore does not resolve horizontal structures.

This paper presents a common volume (CV) comparison of PMC brightness from the AIM CIPS and the Odin OSIRIS experiments. In order to quantitatively compare CIPS and OSIRIS PMC brightness measurements, we choose a suitable CV for overlapping OSIRIS and CIPS observations, define a quantity that is suitable for describing both observations, and correct for differences in scattering conditions, i.e., wavelength and SCA. The uncertainties inherent in the method are described and quantified. This methodology addresses the long-standing issue of making limb and nadir measurements comparable. Section 2 presents the methodology, including the definition of the coincidence criterion (Section 2.1) and the CV (Section 2.2), the choice of comparison quantity (Section 2.3), corrections for differences in scattering conditions (Section 2.4), and the interpretation of data in the CV (Section 2.5). In Section 3 the comparison results are presented and discussed; Section 4 gives a summary.

2. Methodology

We present a comparison of CIPS and OSIRIS observations in two northern hemispheric (NH) PMC seasons 2008 (NH08) and 2009 (NH09). In these two seasons CIPS and OSIRIS PMC observations that are coincident in space and time serendipitously accumulate around 79°N during three, usually 5-day long intervals between June and August of NH08 and NH09 each. In the southern hemisphere (SH), Odin points out of the orbit plane, i.e., OSIRIS looks towards the South Pole rather than along the Odin orbit, so finding coincidences is much more difficult.

2.1. Coincidence criterion

The CIPS and OSIRIS measurements were required to occur within 12 min of one another. Fig. 1 shows one example for the locations of two coinciding OSIRIS and CIPS orbits, as well as the location of the CIPS CV and the OSIRIS observation. Due to the size of a CIPS pixel of 25 km^2, the spatial coincidence occurs within approximately ±5 km.

We do not take into account the increasing width of the OSIRIS field-of-view with distance from the Odin tangent point. This width changes by ~15%, or 4.5 km, from the beginning to the end of the common volume, which is less than the CIPS resolution and thus can be neglected.

2.2. Definition of common volume

In order to make the cloud brightness observations comparable, CIPS albedo must be integrated horizontally and OSIRIS limb radiance must be integrated vertically. Fig. 2 shows the definition of the column volume and the integration limits. The choice of these limits is complicated by the spherical geometry. In particular, a vertical integration of the OSIRIS data is not straight-forward as limb radiances are measured as a function of tangent altitude rather than geometric altitude.

In principle, a retrieval of vertical information from limb measurements is possible by use of appropriate inversion techniques (e.g., Strong et al., 2002). However, in order for these methods to work, one needs to assume that the quantity in question is horizontally homogeneous over a distance covered by the limb measurement. PMCs are highly structured

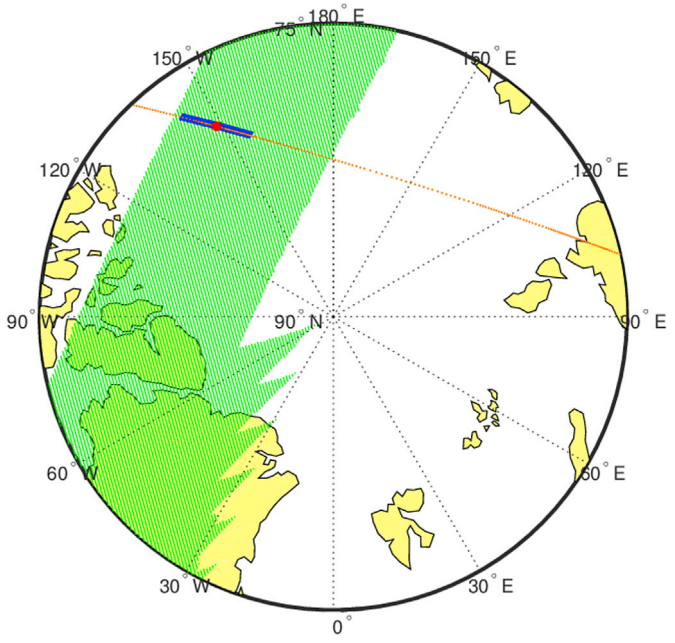

Fig. 1. Example for one coincidence on June 17, 2008. The locations of OSIRIS orbit 39 888 and CIPS orbit 6 235 are shown in orange and green, respectively. The location of the OSIRIS/CIPS CV and the coinciding OSIRIS tangent point are shown in blue and red, respectively. The "sawtooth" structure in part of the CIPS orbit shows the effect of spacecraft rolling during terminator crossings described in Section 2.5. (For interpretation of the references to color in this figure legend, the reader is referred to the Web version of this article.)

and, therefore, often do not allow for a simple inversion. Instead, an integration over the vertical column can be approximated with good accuracy by performing an integration over tangent altitudes with appropriate integration limits. For the OSIRIS PMC observations, a first step is to remove the background profile of molecular Rayleigh scattering (Karlsson and Gumbel, 2005), Reasonable vertical column information can then be obtained by integrating the limb signal from 2.5 km below to 2.5 km above the tangent altitude of maximum limb radiance. This concept has been consolidated by numerically simulating limb integration and true column integration for ensembles of randomly generated PMC fields, allowing for horizontal inhomogeneity in terms of brightness, altitude, and thickness. A detailed description of these studies is in preparation for a separate paper. The results suggest that the above integration limits of ±2.5 km approximate a true column integration averaged over 400 km line-of-sight with an error of less than 10% (standard deviation) for a diverse ensemble of PMC geometries. Sensitivities to the exact choice of integration limits and cloud ensemble are minor. Increasing cloud inhomogeneity generally leads to an increasing statistical uncertainty of inferred column properties, but not to a systematic bias. Fig. 2 illustrates the basic challenge of the vertical limb integration. The cloud volumes denoted as (1) and (2) are within the horizontal limits of the column volume, but are missed by the integration over the limb altitudes. The cloud volumes denoted as (3), on the other hand, contribute to the limb integration although they are outside the horizontal limits of the common volume. For an appropriate choice of limb integration limits, these two effects will largely cancel each other for a wide range of cloud geometries.

The horizontal OSIRIS path of ±200 km defines the integration limits to be applied to the CIPS albedo along the OSIRIS line-of-sight. In addition, the CIPS albedo must be integrated perpendicular to the OSIRIS line-of-sight, since the OSIRIS cross-track field-of-view is ±15 km. In total, the horizontal CIPS integration corresponds to 80 × 6 CIPS pixels of size 25 km^2.

2.3. Choice of comparison quantity

The primary CIPS PMC data product is directional albedo A (sr^{-1}). The primary OSIRIS PMC data product is limb radiance L (photons (ph) cm^{-2} s^{-1} sr^{-1} nm^{-1}). These two quantities are closely tied to the specific observation geometry and are thus difficult to apply to a different geometry. Based on the horizontal and vertical integrations described in Section 2.2, a total PMC-scattered photon intensity (I) from the CV within a given solid angle (ph s^{-1} sr^{-1} nm^{-1}) is defined for both instruments:

$$I_{OSIRIS} = \int_{z_t^*-2.5km}^{z_t^*+2.5km} dz' \int_{-15km}^{15km} dy' L_{277nm}(z_t) \quad (1)$$

$$I_{CIPS} = \int_{-200km}^{+200km} dx' \int_{-15km}^{15km} dy' A_{265nm}^{90°}(x,y) \cdot E_{265nm} \quad (2)$$

$L_{277nm}(z_t)$ is the vertical profile vs. tangent altitude of OSIRIS limb radiance at 277 nm in units of ph cm^{-2} s^{-1} sr^{-1} nm^{-1}, and z_t^* is the tangent altitude of the peak limb radiance in the OSIRIS vertical profile. A is the CIPS directional albedo in units of sr^{-1}, and E_{265nm} is the solar spectral irradiance at 265 nm in units of ph cm^{-2} s^{-1} nm^{-1}. Note that the integration across track in equation (1) is done intrinsically by the OSIRIS instrument integrating radiances over the field-of-view of ±15 km. In equation (2), integration over the same width is then numerically applied to the CIPS data.

2.4. Differences in scattering conditions

The CV quantities I_{OSIRIS} and I_{CIPS} cannot be compared directly as they are based on different scattering conditions. In terms of wavelength, CIPS measures around 265 nm while the shortest wavelengths accessible by OSIRIS are around 277 nm. In terms of phase function, CIPS albedo is normalized to a SCA of 90° while OSIRIS measurements in the CV geometry are performed at SCAs between 72° and 76°. Before the horizontal integration, the albedo values in the individual CIPS pixels are therefore transformed to become comparable to the OSIRIS data. This is done using two transformation factors, C_{spec} and C_{phase}, which correct for

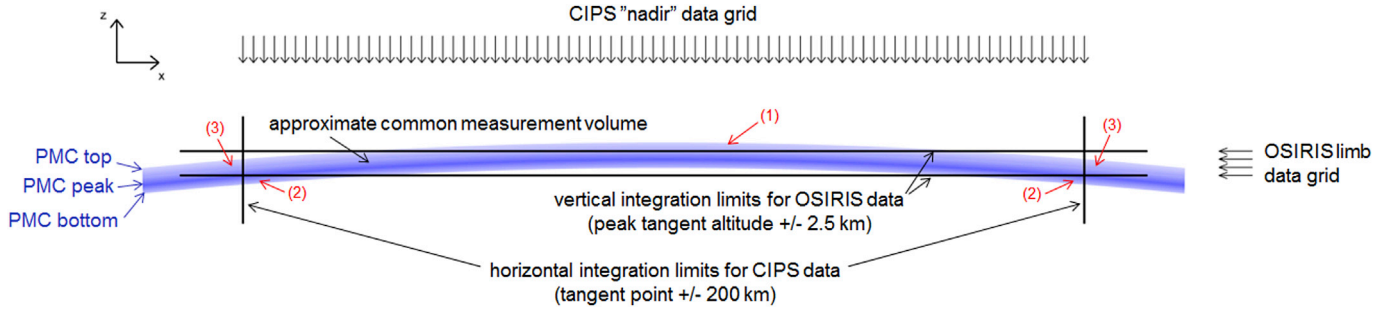

Fig. 2. Geometry and integration limits for the OSIRIS/CIPS CV comparison. Cloud volumes denoted as (1) and (2) are missed by the limb integration, while cloud volumes denoted as (3) contribute to the limb integration although they are outside the horizontal CV limits. For an appropriate choice of limb integration limits, these two effects should largely balance each other. See text for details.

spectral and SCA differences, respectively. These correction factors are dependent on cloud particle size, distribution type and width, particle shape, and particle asphericity. They are obtained from T-matrix simulations (Mishchenko and Travis, 1998; see also Baumgarten et al., 2007) in which the complex refractive index is taken from Warren (1984), and it is assumed that the cloud particles consist of water ice.

The albedo for each individual CIPS pixel is multiplied by the transformation factors corresponding to the cloud particle size for that pixel that was derived in the CIPS retrieval algorithm. The T-matrix simulations are based on the same ice particle assumptions that are used in the operational CIPS retrievals: spheroids with an axial ratio of two, Gaussian size distribution with a distribution width that varies as 0.39 × mode radius for mode radii up to 40 nm and a fixed width of 15.8 nm for larger particles (Lumpe et al., 2013). The resulting modification of equation (2) is

$$I_{CIPS}^{transf} = \int_{-200km}^{+200km} dx' \int_{-15km}^{+15km} dy' C_{phase}(90^\circ \rightarrow 74^\circ) \cdot C_{spec}(265nm \rightarrow 277nm) \cdot A_{265nm}^{90^\circ}(x,y) \cdot E_{277nm} \quad (3)$$

$E_{277nm} = 3.34 \times 1\,0^{13}$ ph cm^{-2} s^{-1} nm^{-1} is the solar irradiance in the spectral interval utilized by the OSIRIS analysis (Chance and Kurucz, 2010). Based on the T-matrix simulations, the above correction factors for a mode radius of e.g. 40 nm are $C_{phase} = 1.47$ and $C_{spec} = 0.87$.

Equation (1) through (3) define a total PMC-scattered photon intensity from the CV in units of photons s^{-1} sr^{-1} nm^{-1}. We can alternatively describe the observations in terms of albedo units (sr^{-1}) by rearranging equations (1) and (3):

$$A_{OSIRIS} = \int_{z_t^*-2.5km}^{z_t^*+2.5km} dz' \int_{-15km}^{+15km} dy' L_{277nm}(z_t) \cdot E_{277nm}^{-1} \times (area\ of\ CIPS\ common\ volume)^{-1} \quad (4)$$

$$A_{CIPS}^{transf} = mean\left(C_{phase}(90^\circ \rightarrow 74^\circ) \cdot C_{spec}(265nm \rightarrow 277nm) \cdot A_{265nm}^{90^\circ}(x,y)\right) \quad (5)$$

In this study the results are shown in units of intensity on the primary axes and in units of albedo on the secondary axes where appropriate.

2.5. The CIPS common volume

This comparison assumes that the CIPS CV is completely filled with finite and valid albedo values. Otherwise, the horizontal integration of CIPS albedo values results in a low bias compared to OSIRIS. Therefore, attention must be paid to any CIPS quality restrictions or missing values in the CV. In the level 2 data product, a quality flag (QF) indicates the quality of the PMC retrieval by referring to the number of different solar zenith angles that have been available for the PMC phase function analysis (Bailey et al., 2009). QF = 0 means six or more measurements; QF = 1 means four or five measurements, and QF = 2 means three or fewer measurements (Lumpe et al., 2013); caution is warranted when using albedo values for which QF = 2. Since the particle radius is in particular adversely affected by an underdetermined phase function, the radius values of pixels with QF = 2 are prefilled with an error code in the CIPS level 2 data. Since a valid radius value is required for the wavelength and phase correction described in Section 2.3, the albedo of any pixel with QF = 2 is set to Not-a-Number (NaN). QF = 2 occurs most often at the cross-track edges of the CIPS orbit where fewer measurements are made of a single location. Furthermore, caution is warranted for cloud pixels with albedo values smaller than 2 × 10^{-6} sr^{-1}, and radius values smaller than 20 nm (Lumpe et al., 2013); we label such pixels as "suspicious" and set the albedo values in them to NaN. In addition, in 2008 and 2009 the spacecraft was rolled during terminator crossings in order for the CIPS and SOFIE instruments to sample the same geographic region. This caused a small fraction of the CIPS pixels to point toward the limb instead of toward nadir; these pixels are assigned values of NaN in the retrieval process. The left-hand panel of Fig. 3 shows the CIPS CV albedo from orbit 6 291 in June 2008. Pixels with QF = 2, 'suspicious' pixels, and limb-pointing pixels are indicated with yellow crosses, green dots, and red crosses, respectively. Considering these colored pixels as invalid, on average over the NH08 and NH09 seasons the percent filling of the CV is 77%; 6% of all CVs are filled completely. The middle panel of Fig. 3 shows the albedo after correction for wavelength and SCA differences as described in Section 2.3. Notice that both the QF = 2 and suspicious pixels are now flagged as NaN. In order to increase the filling of the CIPS CV, a convolution using a 5 × 5 distance-weighted kernel is applied to the missing (NaN) pixels, requiring at least 5 finite pixels. This procedure essentially fills many NaN pixels with the albedo values of surrounding pixels. The result is shown in the right-hand panel of Fig. 3 – note that already existing pixel values have not changed, but missing pixels have been filled in. This procedure increases the mean percentage filling of the CV to 84%, with 16% of all CVs being filled completely with valid cloud data. Nevertheless, missing pixels still skew the integrated CIPS signal low in comparison to the OSIRIS signal. Thus in order to carry out a meaningful comparison of cloud brightness, an assumption about the values of missing pixels is necessary. We calculate the median cloud albedo (excluding non-cloud pixels) in each CIPS CV and use it to fill each missing or invalid CIPS pixel. Realizing that inventing data this way is not ideal, we require that at least 70% of the CIPS CV has to be filled with finite pixels for this study, otherwise those orbits are excluded from the comparison. This requirement reduces the number of coincidences from 232 to 191 (18%).

3. Results and discussion

Fig. 4 shows scatter plots of the CIPS and OSIRIS CV signal, with filled black circles denoting the CV signal values. Red error bars show the CIPS and OSIRIS measurement uncertainties. Dominant contributions to systematic uncertainty of the OSIRIS limb radiances are the absolute calibration of the instrument (~5%), and absorption by an undetermined amount of mesospheric ozone along the optical path (typically 2–5% at PMC altitudes). The combined effect of both is monitored on a climatological basis by analyzing Rayleigh scattering from relevant tangent altitudes during PMC-free conditions. In addition to the resulting systematic uncertainty of about 10%, there is a statistical uncertainty of the measurement, resulting e.g. in a PMC limb radiance detection threshold of about 1 × 10^{9} ph cm^{-2} s^{-1} sr^{-1} nm^{-1} based on the noise level of the molecular scattering background (Karlsson and Gumbel, 2005; Hultgren et al., 2013). In Fig. 4, OSIRIS error bars represent these systematic and statistical uncertainties, the latter after multiplying with the OSIRIS integration area, see Equation (1). An additional statistical uncertainty is introduced when applying vertical integration over tangent altitudes to convert the OSIRIS limb radiances to a CV intensity. As described in Section 2.2, this approximate method of vertical integration introduces an uncertainty (standard deviation) of about 10%. The CIPS random uncertainty of albedo in each pixel is 1e-6 sr^{-1} (Lumpe et al., 2013; their Fig. 21 and discussion thereof). A CIPS negative bias of ~0.5e-6 sr^{-1} connected to observations at the solar zenith angles of our coincidences (60°–70°) is corrected in each CIPS pixel according to Lumpe et al. (2013, their Fig. 21 and discussion thereof).

The double-logarithmic axes in Fig. 4a emphasize a disagreement at very small photon intensity values, for which CIPS measures smaller values than OSIRIS. This concerns roughly a third of the coincidences and

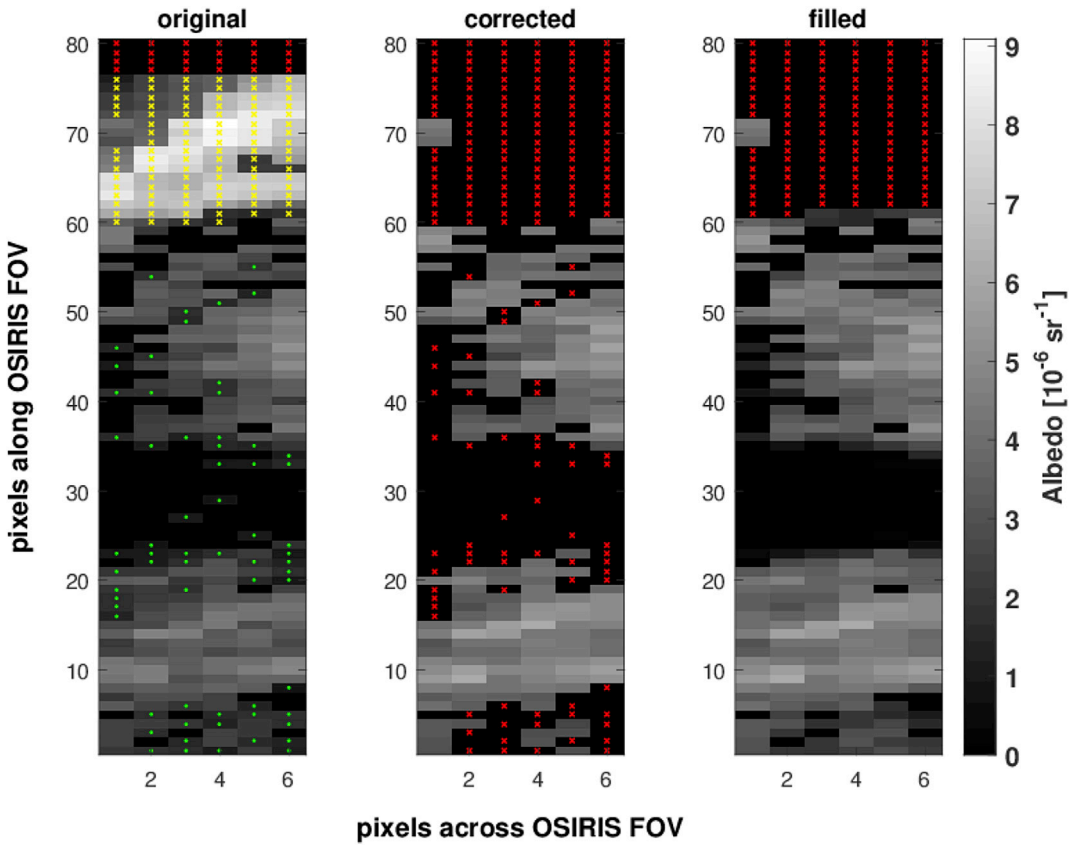

Fig. 3. CIPS CV albedo from orbit 6 291 in June 2008. Left: original CIPS albedo, middle: albedo after wavelength and SCA transformations were applied, right: albedo after filling non-finite pixels with surrounding pixel values (see text). Red crosses denote CIPS pixels filled with NaN, yellow crosses pixels with a QF value of two, and green circles suspicious pixels (see text). In original data, pixels are filled with NaN for out-of-orbit data. (For interpretation of the references to color in this figure legend, the reader is referred to the Web version of this article.)

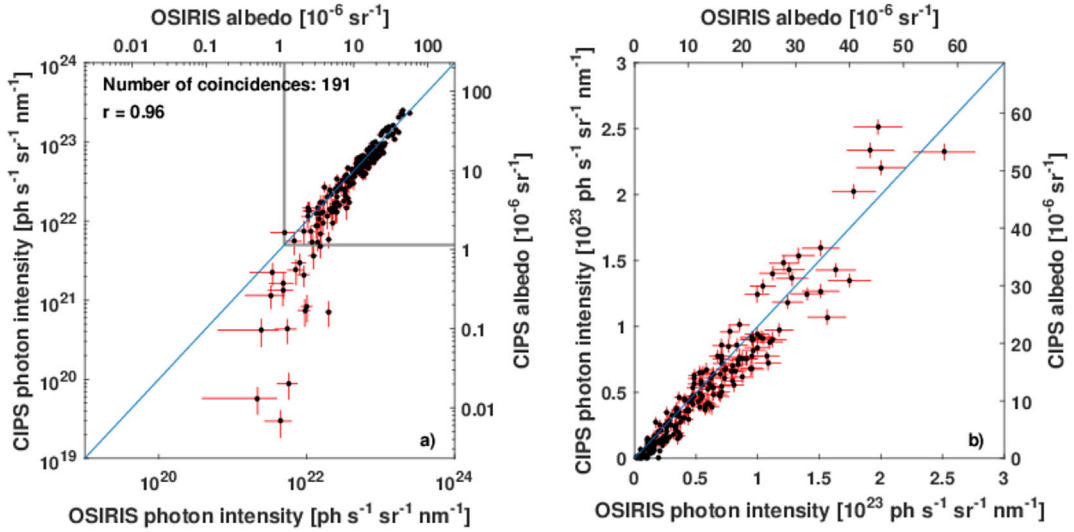

Fig. 4. Scatter plots of CIPS and OSIRIS CV signal, a): double logarithmic, b): linear. The results are shown in units of ph s^{-1} sr^{-1} nm^{-1} (left/bottom axes, equations (1) and (3)) and in units of sr^{-1} (right/top axes, equations (4) and (5)). The red bars denote the CIPS and OSIRIS measurement uncertainties. The blue line shows the one-to-one correlation. The grey lines depict the axis ranges of Fig. 6a. (For interpretation of the references to color in this figure legend, the reader is referred to the Web version of this article.)

is reflected in the mean relative difference between CIPS and OSIRIS of $-102 \pm 55\%$. This value includes the measurement uncertainty depicted by the red error bars. The *mean relative* difference is large because it emphasizes the small number of low photon intensity cases. On the other hand, using the *relative mean* difference, the agreement is $-9 \pm 14\%$. This shows that the instruments agree on average, however, disagree for low cloud photon intensity coincidences. Despite this disagreement, however, the correlation coefficient r = 0.96 is quite high, indicating good agreement overall.

As a nadir-viewing imager, CIPS observes a large number of horizontal pixels, while the limb-viewing OSIRIS instrument provides height-resolved but coarser observations integrated over a longer path. Owing to

these different observation geometries, OSIRIS provides higher sensitivity to PMCs in its field-of-view than CIPS can provide in its individual image pixel. For CIPS, PMCs appear as small enhancements of the bright background (Rayleigh scattering) signal. OSIRIS observes the Earth's limb, where the Rayleigh background is not as bright as in the nadir. Furthermore, OSIRIS integrates the cloud signal over a much longer line of sight (~400 km) than the vertically observing CIPS. Thus OSIRIS can observe fainter clouds than CIPS. Therefore, we expect differences between the cloud retrievals for very faint clouds: it is possible that the CIPS retrieval algorithm reports the absence of a cloud, i.e., a cloud albedo of zero, in cases where there is a very faint cloud present that OSIRIS is able to observe. This phenomenon is quantified by Lumpe et al. (2013), their Fig. 18, which shows the CIPS cloud detection sensitivity vs. Solar Zenith Angle (SZA) for different cloud albedo values, based on simulated retrievals. In our study the CIPS CV SZA ranges from 60° to 71°. In this range 40–60% of 2G clouds, 65–80% of 3G clouds, and 85–90% of 4G clouds are reported as clouds by CIPS. Including these zero albedo pixels in the CV then results in an underestimate of the CIPS CV signal relative to OSIRIS. This CIPS underestimate should be more noticeable when more zero-cloud pixels are present in the CIPS CV. Fig. 5 shows the relative difference in CV signal between the two instruments vs. the percent filling of the CIPS CV with pixels that have non-zero albedo values. The CIPS low bias increases to around 200% as the number of pixels with non-zero albedo decreases; the percent differences approach zero for higher numbers of non-zero pixels, as expected from the described sensitivity difference.

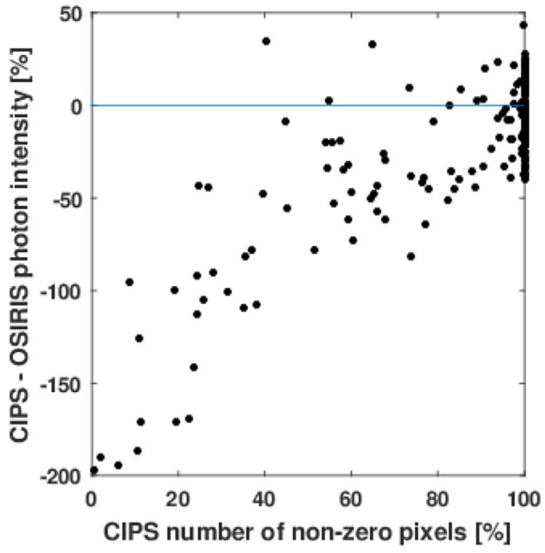

Fig. 5. Relative difference in CV signal (2*(CIPS - OSIRIS)/(CIPS + OSIRIS)) vs. percentage of CIPS pixels in CV with non-zero albedo pixels.

This sensitivity issue can be avoided in the comparison by including only coincidences for which the CIPS CV is mostly filled with non-zero albedo pixels. Requiring a filling of 95% or more reduces the number of coincidences further from 191 to 120, removing 71 coinciding orbits from the analysis. Fig. 6 corresponds to Fig. 4, but shows results only for coincidences for which the CIPS CV is filled at least 95% with non-zero cloud pixels. Thus the low-signal measurements where CIPS is systematically lower than OSIRIS are not present in this figure. With this adjustment, the mean relative difference (relative mean difference) reduces to $-6 \pm 14\%$ ($-4 \pm 13\%$), which is now within the uncertainty of the mean. The correlation coefficient decreases very slightly to 0.94, which is still quite remarkable.

Retrieval uncertainties caused by the inhomogeneous and variable nature of PMCs will contribute to the scatter in the cloud brightness comparison in Fig. 6. Many studies have shown that PMCs vary on scales from a few km to hundreds of km (e.g., Gadsden and Parviainen, 1996; Chandran et al., 2009; Rusch et al., 2009; Thurairajah et al., 2013). As described above, inhomogeneity issues that have been addressed in the current study are related to the approximated vertical limb integration for OSIRIS, and to the cloud-filling for CIPS. Fig. 7, which relates the relative difference (CIPS− OSIRIS) in cloud brightness to the inhomogeneity in the CIPS CV, shows that the differences in fact vary systematically with level of inhomogeneity: the inhomogeneity is greatest at small fill factors, i.e. large regions where CIPS does not observe clouds. It is possible that the CIPS sensitivity issue described above completely accounts for this finding. On the other hand, using the results of this study alone, we cannot exclude that this behavior is also influenced by effects of PMC inhomogeneity on the OSIRIS observations. This means that we cannot distinguish between the effects of dim clouds (small fill factors), which lead to a low bias in CIPS, and inhomogeneity, which may lead to uncertainty in the OSIRIS results. This limitation is certainly also true when comparing other nadir/limb combinations than the one presented in this study. While CIPS has the finest horizontal resolution of all current PMC-observing nadir instruments, other nadir instruments could potentially be used in similar studies, as long as the nadir pixel or footprint size is sufficiently small compared to specific limb

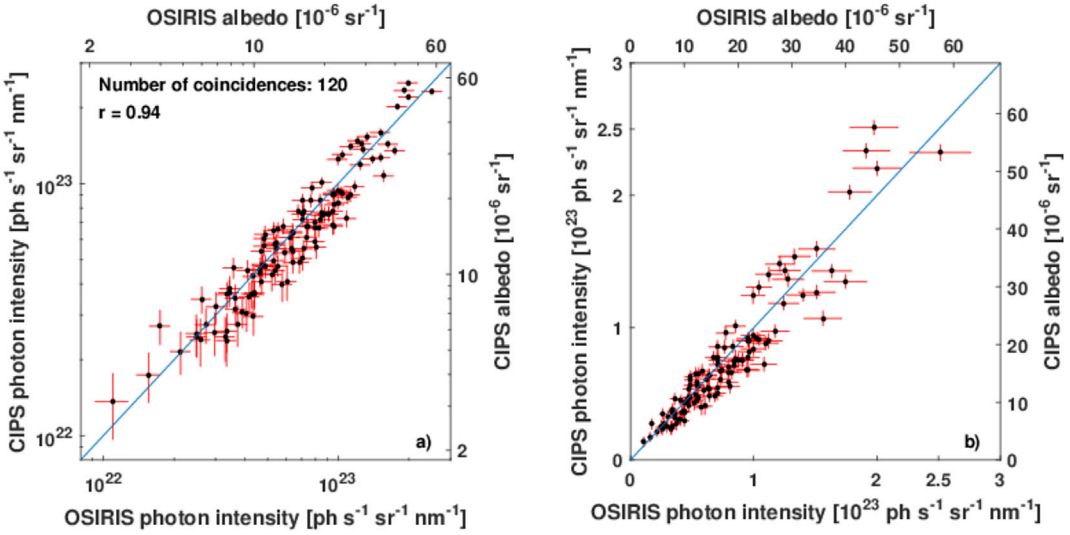

Fig. 6. Same as Fig. 4, but using only coincidences for which the CIPS CV is filled at least 95% with pixels that have a non-zero albedo value. Note the changed axis ranges in Fig. 6a compared to Fig. 4a as shown by grey lines in Fig. 4a.

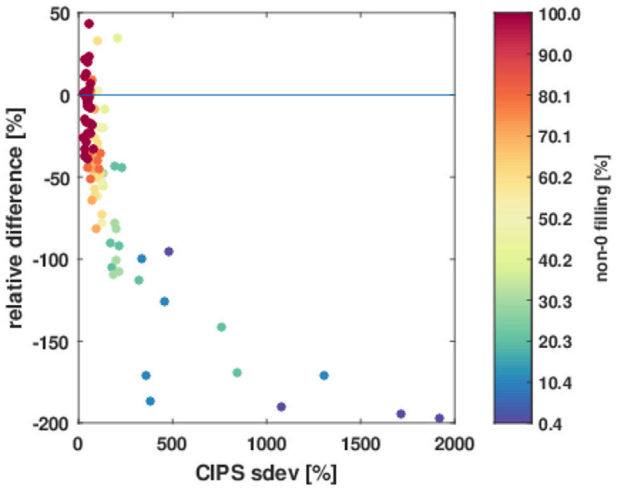

Fig. 7. Relative difference (CIPS− OSIRIS) in cloud brightness vs. the relative albedo standard deviation in the CIPS CV. The points are color-coded in terms of the filling-percentage of the common-volume with non-zero albedo pixels. (For interpretation of the references to color in this figure legend, the reader is referred to the Web version of this article.)

observation volumes.

As described in Section 2.2, the choice of the common volume is not trivial: we must fit a curved cloud layer into a rectangular volume, which in turn leads to assumptions about vertical and horizontal integration limits. These choices are obviously not ideal for every cloud situation, but resemble the overall general behavior of a cloud layer to the best of our knowledge. The fact that, on average, the agreement in cloud brightness is within the uncertainty of the mean, tells us that we have chosen a reasonable definition of the CIPS-OSIRIS CV. Having this established, a path is now open for further CV comparison of CIPS and OSIRIS in terms of PMC ice water content or particle sizes. CV studies combining different satellite instruments can provide important keys to ongoing discussions about particle size distributions and PMC evolution. This will also comprise detailed comparisons between CIPS and special OSIRIS tomography scans (Hultgren and Gumbel, 2014). Winds can potentially move clouds into and out of the CV within a few minutes, and microphysics can occur on scales of minutes (Baumgarten et al., 2012). Using our temporal coincidence criterion of 12 min and assuming a mean wind of 25 m/s (e.g., Fig. 2 in Hall et al. (2003)), a cloud moves, on average, 18 km during that time. The typical summer wind below the mesopause is directed west-southwest (Hall et al., 2003), which is nearly perpendicular to the Odin orbit. This means that the PMC can almost completely leave or enter the width of the OSIRIS field of view of ~30 km during 12 min. However, constraining the coincidences to a smaller time difference does not improve the scatter in the data points (not shown). We conclude therefore that the effect of transport of clouds into and out of the CV averages out during the two seasons and does not affect this comparison.

4. Summary

This paper describes the comparison of PMC brightness from CIPS nadir observations to OSIRIS limb observations. This study addresses the long-standing issue of making limb and nadir measurements comparable: it defines a CV for overlapping OSIRIS and CIPS observations as well as a photon scattering intensity quantity that is suitable for jointly describing nadir and limb observations, and corrects for different scattering conditions such as wavelength and SCA differences. The 191 coincidences of cloud brightness are very highly correlated, with $r = 0.96$. The mean relative difference (CIPS - OSIRIS) is $-102 \pm 55\%$. The relative difference depends strongly on the number of pixels in the CV that CIPS reports as zero cloud albedo, with very large (up to 200%) differences for coincidences that are mostly filled with such non-cloud pixels. This strongly indicates that one contribution to the differences between CIPS and OSIRIS is the lower CIPS sensitivity compared to OSIRIS: a cloud that OSIRIS observes as a faint cloud may have an albedo value that is below the detection threshold for CIPS; therefore, that cloud may be reported as a non-cloud pixel by CIPS. In a CV with many faint clouds, this would result in the CIPS CV signal being lower than the OSIRIS signal. Other contributions could be biases in the OSIRIS retrievals caused by the choice of the CV or by inhomogeneities along the line of sight, which are larger in the partially filled CV comparisons. Comprehensive simulations have been performed to characterize these effects on the OSIRIS limb analysis, and will be described in an upcoming paper. By only including coincidences for which the filling of the CIPS CV with non-zero clouds pixels is at least 95%, the CIPS-OSIRIS differences are substantially reduced. The remaining 120 coincidences show agreement in cloud brightness of $-6 \pm 14\%$, with a very strong correlation of $r = 0.94$. A possible effect on these results of winds transporting clouds into and out of the CV is considered but found insignificant. The agreement in cloud brightness retrieved by CIPS and OSIRIS using very different retrieval approaches and observation geometries is very encouraging for future inter-satellite comparisons, as well as for future comparisons of ice water content and particle radii.

Acknowledgements

Odin is a Swedish-led satellite funded jointly by Sweden (SNSB), Canada (CSA), France (CNES), and Finland (TEKES). Since April 2007, Odin is a third-party mission of the European Space Agency. Funding for CIPS data evaluation and the AIM mission was provided by the NASA Small Explorer program under contract NAS5–03132. We thank the LASP data system team for processing the AIM CIPS data, and Gary Thomas for helpful discussions.

References

Andrews, D.G., Holton, J.R., Leovy, C.B., 1987. Middle Atmosphere Dynamics. Academic Press, San Diego.

Backhouse, T.W., 1885. The luminous cirrus clouds of June and July. Meteorol. Mag. 20, 133.

Bailey, S.M., Merkel, A.W., Thomas, G.E., Carstens, J.N., 2005. Observations of Polar Mesospheric Clouds by the student nitric oxide explorer. J. Geophys. Res. 110 (D13) https://doi.org/10.1029/2004JD005422.

Bailey, S.M., Thomas, G.E., Rusch, D.W., Merkel, A.W., Jeppesen, C.D., Carstens, J.N., Randall, C.E., McClintock, W.E., Russell III, J.M., 2009. Phase functions of polar mesospheric cloud ice as observed by the CIPS instrument on the AIM satellite. J. Atmos. Sol.-Terr. Phys. 71, 373–380. https://doi.org/10.1016/j.jastp.2008.09.039.1.

Bailey, S.M., Thomas, G.E., Hervig, M.E., Lumpe, J.D., Randall, C.E., Carstens, J.N., Thurairajah, B., Rusch, D.W., Russell III, J.M., Gordley, L.L., 2015. Comparing nadir and limb observations of polar mesospheric clouds: the effect of the assumed particle size distribution. J. Atmos. Sol.-Terr. Phys. 127, 51–65. https://doi.org/10.1016/j.jastp.2015.02.007.

Baumgarten, G., Fiedler, J., Von Cossart, G., 2007. The size of noctilucent cloud particles above ALOMAR (69N,16E): optical modeling and method description. Adv. Space Res. 40 (6), 772–784. https://doi.org/10.1016/j.asr.2007.01.018.

Baumgarten, G., Chandran, A., Fiedler, J., Hoffmann, P., Kaifler, N., Lumpe, J.D., Merkel, A.W., Randall, C.E., Rusch, D.W., Thomas, G.E., 2012. On the horizontal and temporal structure of noctilucent clouds as observed by satellite and lidar at ALOMAR (69N). Geophys. Res. Lett. 39 https://doi.org/10.1029/2011GL049935.

Benze, S., Randall, C.E., DeLand, M.T., Thomas, G.E., Rusch, D.W., Bailey, S.M., Russell III, J.M., McClintock, W.E., Merkel, A.W., Jeppesen, C.D., 2009. Comparison of polar mesospheric cloud measurements from the cloud imaging and particle size experiment and the solar backscatter ultraviolet instrument in 2007. J. Atmos. Sol.-Terr. Phys. 71, 365–372. https://doi.org/10.1016/j.jastp.2008.07.014.

Benze, S., Randall, C.E., DeLand, M.T., Thomas, G.E., Bailey, S.M., Russell III, J.M., Merkel, A.W., 2011. Evaluation of AIM CIPS measurements of polar mesospheric clouds by comparison with SBUV data. J. Atmos. Sol. Terr. Phys. 73, 2065–2072. https://doi.org/10.1016/j.jastp. 2011.02.003.

Chance, K., Kurucz, R.L., 2010. An improved high-resolution solar reference spectrum for earth's atmosphere measurements in the ultraviolet, visible, and near infrared. J. Quant. Spectrosc. Radiat. Transfer 111, 1289–1295. https://doi.org/10.1016/j.jqsrt.2010.01.036.

Chandran, A., Rusch, D.W., Palo, S.E., Thomas, G.E., Taylor, M.J., 2009. Gravity wave observations in the summertime polar mesosphere from the Cloud Imaging and

Particle Size (CIPS) experiment on the AIM spacecraft. J. Atmos. Sol.-Terr. Phys. 71, 392–400. https://doi.org/10.1016/j.jastp.2008.09.041.
DeLand, M.T., Shettle, E.P., Thomas, G.E., Olivero, J.J., 2003. Solar backscattered ultraviolet (SBUV) observations of polar mesospheric clouds (PMCs) over two solar cycles. J. Geophys. Res. 108 (D8), 8445. https://doi.org/10.1029/2002JD002398.
Gadsden, M., Parviainen, P., 1996. Observing Noctilucent Clouds. International Association of Geomagnetism and Aeronomy available on. http://www.iaga-aiga.org/data/uploads/pdf/guides/onc.pdf.
Garcia, R.R., 1989. Dynamics, radiation, and photochemistry in the mesosphere - implications for the formation of noctilucent clouds. J. Geophys. Res. 94 (D12), 14605–14615. https://doi.org/10.1029/JD094iD12p14605.
García-Comas, M., López-Puertas, M., Funke, B., Jurado-Navarro, Á.A., Gardini, A., Stiller, G.P., von Clarmann, T., Höpfner, M., 2016. Measurements of global distributions of polar mesospheric clouds during 2005-2012 by MIPAS/Envisat. Atmos. Chem. Phys. 16, 6701–6719. https://doi.org/10.5194/acp-16-6701-2016.
Gordley, L.L., Hervig, M.E., Fish, C., Russell III, J.M., Bailey, S., Cook, J., Hansen, S., Shumway, A., Paxton, G., Deaver, L., Marshall, T., Burton, J., Magill, B., Brown, C., Thompson, E., Kemp, J., 2009. The solar occultation for ice experiment. J. Atmos. Sol. Terr. Phys. 71, 3–4. https://doi.org/10.1016/j.jastp.2008.07.012, 300-315.
Hall, C.M., Aso, T., Manson, A.H., Meek, C.E., Nozawa, S., Tsutsumi, M., 2003. High-latitude mesospheric mean winds: a comparison between Tromsø (69°N) and Svalbard (78°N). J. Geophys. Res. 108 (D19) https://doi.org/10.1029/2003JD003509.
Hervig, M., Siskind, D., 2006. Decadal and inter-hemispheric variability in polar mesospheric clouds, water vapor, and temperature. J. Atmos. Sol.-Terr. Phys. 68 (1), 30–41. https://doi.org/10.1016/j.jastp.2005.08.010.
Hultgren, K., Gumbel, J., 2014. Tomographic and spectral views on the lifecycle of polar mesospheric clouds from Odin/OSIRIS. J. Geophys. Res. 119, 14129–14143. https://doi.org/10.1002/2014JD022435.
Hultgren, K., Gumbel, J., Degenstein, D., Bourassa, A., Lloyd, N., Stegman, J., 2013. First simultaneous retrievals of horizontal and vertical structures of Polar Mesospheric Clouds from Odin/OSIRIS tomography. J. Atmos. Sol. Terr. Phys. 104, 213–223. https://doi.org/10.1016/j.jastp.2013.06.013.
Jesse, O., 1885. Auffallende abenderscheinungen am himmel. Meteor. Z. 2, 311–312.
Karlsson, B., Gumbel, J., 2005. Challenges in the limb retrieval of noctilucent cloud properties from ODIN/OSIRIS. Adv. Space Res. 36, 935–942. https://doi.org/10.1016/j.asr.2005.04.074.
Leslie, R.C., 1885. Sky glows. Nature 32. https://doi.org/10.1038/032245a0.
Llewellyn, E.J., et al., 2004. The OSIRIS instrument on the Odin spacecraft. Can. J. Phys. 82, 411–422. https://doi.org/10.1139/p04-005.
Lübken, F.J., Berger, U., Baumgarten, G., 2009. Stratospheric and solar cycle effects on long-term variability of mesospheric ice clouds. J. Geophys. Res. 114 https://doi.org/10.1029/2009JD012377.
Lumpe, J.D., Alfred, J.M., Shettle, E.P., Bevilacqua, R.M., 2008. Ten years of southern hemisphere polar mesospheric cloud observations from the polar ozone and Aerosol measurement instruments. J. Geophys. Res. 113 (D04205) https://doi.org/10.1029/2007JD009158.
Lumpe, J.D., Bailey, S.M., Carstens, J.N., Randall, C.E., Rusch, D.W., Thomas, G.E., Nielsen, K., Jeppesen, C., McClintock, W.E., Merkel, A.W., Riesberg, L., Templeman, B., Baumgarten, G., Russell III, J.M., 2013. Retrieval of polar mesospheric cloud properties from CIPS: algorithm description, error analysis and cloud detection sensitivity. J. Atmos. Sol.-Terr. Phys. 104, 167–196. https://doi.org/10.1016/j.jastp.2013.06.007.
McClintock, W.E., Rusch, D.W., Thomas, G.E., Merkel, A.W., Lankton, M.R., Drake, V.A., Bailey, S.M., Russell III, J.M., 2009. The cloud imaging and particle size experiment on the Aeronomy of Ice in the mesosphere mission: instrument concept, design, calibration, and on-orbit performance. J. Atmos. Sol.-Terr. Phys. 71, 340–355. https://doi.org/10.1016/j.jastp.2008.10.011.
Mishchenko, M.I., Travis, L.D., 1998. Capabilities and limitations of a current FORTRAN implementation of the T-matrix method for randomly oriented, rotationally symmetric scatterers. J. Quantitative Spectrosc. Radiat. Transf. 60, 309–324. https://doi.org/10.1016/S0022-4073(98)00008-9.
Murtagh, D., et al., 2002. An overview of the Odin atmospheric mission. Can. J. Phys. 80, 309–319. https://doi.org/10.1139/P01-157.
Robert, C.E., von Savigny, C., Rahpoe, N., Bovensmann, H., Burrows, J.P., DeLand, M.T., Schwartz, M.J., 2010. First evidence of a 27 day solar signature in noctilucent cloud occurrence frequency. J. Geophys. Res.-Atmos. 115 https://doi.org/10.1029/2009JD012359.
Rusch, D.W., Thomas, G.E., McClintock, W., Merkel, A.W., Bailey, S.M., Russell III, J.M., Randall, J.M., Jeppesen, C.D., Callan, M., 2009. The cloud imaging and particle size experiment on the aeronomy of ice in the mesosphere mission: cloud morphology for the northern 2007 season. J. Atmos. Sol.-Terr. Phys. 71, 356–364. https://doi.org/10.1016/j.jastp.2008.11.005.
Russell III, J.M., Bailey, S.M., Gordley, L.L., Rusch, D.W., Horanyi, M., Hervig, M.E., Thomas, G.E., Randall, C.E., Siskind, D.E., Stevens, M.H., Summers, M.E., Taylor, M.J., Englert, C.R., Espy, P.J., McClintock, W.E., Merkel, A.W., 2009. The Aeronomy of Ice in the Mesosphere (AIM) mission: overview and early science results. J. Atmos. Sol.-Terr. Phys. 71, 289–299, 0.1016/j.jastp.2008.08.011.
Schröder, W., 2003. Comment on "are noctilucent clouds truly a "Miner's canary" for global Change?". Eos Trans. AGU, 2003 84 (37), 365. https://doi.org/10.1029/2003EO370008.
Shepherd, T.G., 2000. The middle atmosphere. J. Atmos. Sol.-Terr. Phys. 62, 1587–1601. https://doi.org/10.1016/S1364-6826(00)00114-0.
Siskind, D.E., Drob, D.P., Emmert, J.T., Stevens, M.H., Sheese, P.E., Llewellyn, E.J., Hervig, M.E., Niciejewski, R., Kochenash, A.J., 2012. Linkages between the cold summer mesopause and thermospheric zonal mean circulation. Geophys. Res. Lett. 39, 1. https://doi.org/10.1029/2011GL050196.
Strong, K., Joseph, B.M., Dosanjh, R., McDade, I.C., McLinden, C.A., McConnell, J.C., Stegman, J., Murtagh, D.P., Llewellyn, E.J., 2002. Retrieval of vertical concentration profiles from OSIRIS UV-visible limb spectra. Can. J. Phys. 80, 409–434. https://doi.org/10.1139/P01-153.
Thomas, G.E., 1984. Solar mesosphere explorer measurements of polar mesospheric clouds (noctilucent clouds). J. Atmos. Terr. Phys. 46 (9), 819–824. https://doi.org/10.1016/0021-9169(84)90062-X.
Thomas, G.E., 1996. Is the polar mesosphere the miner's canary of global change? Adv. Space Res. 18 (3), 149–158. https://doi.org/10.1016/0273-1177(95)00855-9.
Thomas, R.J., Donahue, T.M., 1972. Analysis of OGO-6 observations of oi5577-a tropical nightglow. J. Geophys. Res. 77, 3557–3565. https://doi.org/10.1029/JA077i019p03557.
Thomas, G.E., McPeters, R.D., Jensen, E.J., 1991. Satellite-observations of polar mesospheric clouds by the solar backscattered ultraviolet spectral radiometer - evidence of a solar-cycle dependence. J. Geophys. Res. 96 (D1), 927–939. https://doi.org/10.1029/90JD02312.
Thomas, G.E., Olivero, J.J., Deland, M.T., Shettle, E.P., 2003. Comment on “are noctilucent clouds truly a “Miner's canary” for global Change?”. Eos Trans. AGU 84 (36), 352–353. https://doi.org/10.1029/2003EO360008.
Thurairajah, B., Bailey, S.M., Nielsen, K., Randall, C.E., Lumpe, J.D., Taylor, M.J., Russell III, J.M., 2013. Morphology of polar mesospheric clouds as seen from space. J. Atmos. Sol.-Terr. Phys. 104, 234–243. https://doi.org/10.1016/j.jastp.2012.09.009.
von Savigny, C., Petelina, S.V., Karlsson, B., Llewellyn, E.J., Degenstein, D.A., Lloyd, N.D., Burrows, J.P., 2005. Vertical variation of NLC particle sizes retrieved from Odin/OSIRIS limb scattering observations. Geophys. Res. Lett. 32, L07806 https://doi.org/10.1029/2004GL021982.
von Zahn, U., 2003. Are noctilucent clouds a “Miner's Canary” for global change? Eos Trans. AGU 84 (28), 261–264. https://doi.org/10.1029/2003EO280001.
Warren, S.G., 1984. Optical constants of ice from the ultraviolet to the microwave. Appl. Opt. 23 (8), 1206–1225. https://doi.org/10.1364/AO.23.001206.